Structures 14 (2018) 56–68

Contents lists available at ScienceDirect

Structures

journal homepage: www.elsevier.com/locate/structures

On Structural Behavior of a Funicular Concrete Polyhedral Frame Designed by 3D Graphic Statics

Mohammad Bolhassani[a], Masoud Akbarzadeh[a,*], Mehrad Mahnia[b], Ramtin Taherian[b]

[a] Polyhedral Structures Laboratory, School of Design, University of Pennsylvania, Philadelphia, USA
[b] The Alliance Co., Tehran, Iran

ARTICLE INFO

Keywords:
Funicular polyhedral frame
Spatial prefab concrete
Finite element analysis
3D graphic statics
Polyhedral reciprocal diagrams
Combined compression and tension members
Concrete damage plasticity

ABSTRACT

This paper investigates the mechanical behavior of the first built funicular structure designed by 3D graphic statics (3DGS) using reciprocal polyhedral diagrams. Graphic statics methods are unique among other structural design techniques in providing an intuitive control over the form of the structure and its equilibrium of forces for designers. Since graphic statics does not include material properties in the form finding process, further numerical investigations to foresee the behavior of the system under loading scenarios other than the 3DGS design loads are unavoidable. This research reports the structural behavior of Hedracrete which is a prefab, concrete, polyhedral frame with both compression and tension members. A simplified (bar-node) and a detailed volumetric mesh model of the structure are numerically analyzed under eight different loading scenarios. Different combinations of linear and nonlinear material behavior for steel and concrete in addition to linear and quadratic element types are used in those analyses. The analyses are planned to initially verify the equilibrium results of the 3DGS model and to predict the maximum load-bearing capacity of the structure by studying the failure mechanism of the system.

1. Introduction

Geometric structural design methods, known as graphic statics (GS), are considered among the most powerful design techniques that have been researched and practiced by many researchers and structural designers since the early nineteenth century [3,9,12,13,16,18,21,22,26]. Graphical methods, either used as procedural techniques or implemented computationally, result in structural concepts that are exemplary of structural efficiency and expressive form.

What makes GS methods unique among other structural design techniques is the unprecedented and intuitive control that it provides for designers; in GS, the form of the structure and its equilibrium of forces are represented by two diagrams known as *form* and *force* diagrams. These diagrams are *reciprocal* [18]; i.e. geometrically and topologically dependent. Thus, a change in one diagram results in a change in the other. This unique property allows designers to explicitly control the form of the structure as well as the magnitude of its internal and external forces.

1.1. Graphic statics: a brief development history

GS methods fall into three main categories; 2D, 2.5D, and 3DGS methods; 2DGS methods that are based on 2D reciprocal diagrams were originally proposed by Rankine [23], formulated by Maxwell [18] and developed by Culmann [13], Cremona [12], and many others [28]. Although their resulting structural forms are limited to 2D concepts, 2DGS methods were used by many eminent engineers and designers such as Guastavino, Maillart, Eiffel, Nervi, Dieste and their built structures are highly commended for their minimal use of materials [8,14].

Thrust Network Analysis (TNA) [10] is an example of the 2.5GS method combining 2D polygonal reciprocal diagrams and force density method [25] to generate breathtaking, funicular free-form shells which are generated/represented as height fields [27].

There are multiple extensions of GS in three dimensions; the methods that are based on i) projective geometry; ii) reciprocal (non-planar) polygonal diagrams and iii) reciprocal polyhedral diagrams. The methods that are based on projective geometry were mainly developed by Föpl [15] and can be used to analyze determinate 3D truss systems, but the complexity of the projective drawings can make it quite counter-intuitive for designers.

The GS method based on reciprocal (non-planar) polygonal diagrams was proposed by Maxwell [18] and Cremona [12] and the use of these methods based on Combinatorial Equilibrium Modelling (CEM)

* Corresponding author.
E-mail addresses: mb3238@upenn.edu (M. Bolhassani), masouda@upenn.edu (M. Akbarzadeh).

https://doi.org/10.1016/j.istruc.2018.02.002
Received 30 November 2017; Received in revised form 2 February 2018; Accepted 2 February 2018
Available online 12 February 2018
2352-0124/

Fig. 1. A photograph of the built structure in Sa'dabad Complex, Tehran, Iran.

has recently been suggested by Ohlbrock et al. [21].

3D Graphic Statics Using Polyhedral Reciprocal Diagrams is the third category and will be referred to 3DGS in this paper. This method has recently been developed based on a 150-year-old proposition in Philosophical Magazine by Rankine [23], Akbarzadeh [2], Akbarzadeh et al. [4], and McRobie et al. [20]. As shown in Fig. 2, in 3DGS, the equilibrium of a node v_i of a polyhedral frame and its connected members/applied force(s) $e_{i,j}$ is represented by a closed polyhedral cell c_i whose faces are perpendicular to the members/applied force(s) of the node. The magnitude of the internal force $\mathbf{f}_{i,j}$ in each member is equal to the area of the corresponding face $f_{i,j}$ in the polyhedral cell [4]. In the following paragraphs, the form finding, materialization, and construction of this structure will be briefly explained to provide a foundation for further investigation in this paper.

1.2. Hedracrete: funicular polyhedral concrete

Hedracrete is a prefabricated, concrete polyhedral frame and the first built structure designed by the use of 3D graphic statics based on reciprocal polyhedral diagrams [2]. The form of the structure is a funicular polyhedral frame comprised of both compression-only and tensile-only members with the total height of 3.33 m, spanning from three supports located 5.4 m apart from each other. The structure consists of 129 prefabricated parts, 45 joints, 54 compression and 30 tension members sitting on steel supports connected by steel rods (Figs. 1 and 3). All parts were constructed from Glass Fiber Reinforced Concrete (GFRC) except the steel supports and the connectors of the tensile members. The total weight of the structure is 5480.6 kg where the heaviest joint and member weigh 103.8 kg and 126.8 kg, respectively [7].

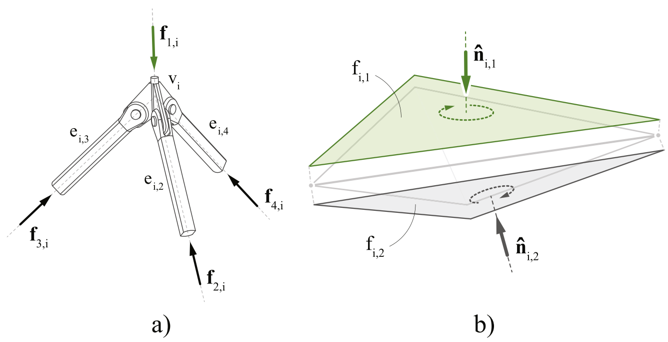

Fig. 2. (a) Node v_i of a spatial structure in equilibrium; and (b) the elements of the reciprocal cell c_i representing the equilibrium of node v_i, with directions of normals of the faces $f_{i,1}$.

1.3. Problem statement and objectives

Although 3DGS allows exploring static equilibrium of variety of non-conventional funicular solutions in three dimensions, its does not include material properties and self-weight of the members. Therefore, the mechanical behavior of the spatial funicular forms design by 3DGS must be evaluated using additional analytical models based on the assigned material properties and various loading cases other than the 3DGS design loads.

Hedracrete is the first application of 3DGS in constructing audacious spatial concrete structures. Thus, further investigations must be conducted to understand and predict the mechanical behavior of such systems. Consequently, this research sets a twofold objective:

- to validate the results of the applied 3DGS using numerical calculations;
- to investigate and predict the mechanical behavior of the built structure such as the type and magnitude of the internal stresses under its self-weight, ultimate load bearing capacity, and failure mechanism.

The following sections will expand on the structural form finding and fabrication process of Hedracrete followed by numerical analysis setup and the results for this funicular polyhedral frame.

2. Structural form finding

The development process of the form finding including the main idea and its development was explained thoroughly in Akbarzadeh et al. [7], and in this paper, we briefly explain the outcomes of the form finding process. The main objective in the form finding process was to find a *spatial* funicular form with both compression and tension members. There are some historic examples of expressive structures designed by 2DGS methods that are exemplary of the innovative use of material, construction technique and efficiency. However, their geometry is an extrusion of a 2D concept. Maillart's Chiasso Shed is an excellent example of such structures with both compression and tension members made out of concrete [29] (Fig. 4).

In 3DGS, the equilibrium of the external forces, which includes the applied and reaction forces, is controlled by the closeness of the Global Force Polyhedron (GFP) in the force diagram, and, the equilibrium of each node within the structure is represented by the closeness of a Nodal Force Polyhedron (NFP) [4,6]. As a rule of thumb, in a force diagram, if all NFPs are convex and contained within the volume of a GFP, there exists a form configuration with compression/tension-only members [3]. Whereas, if the volume of GFP does not contain all NFPs, there is a form configuration with both compressive and tensile forces [2,17].

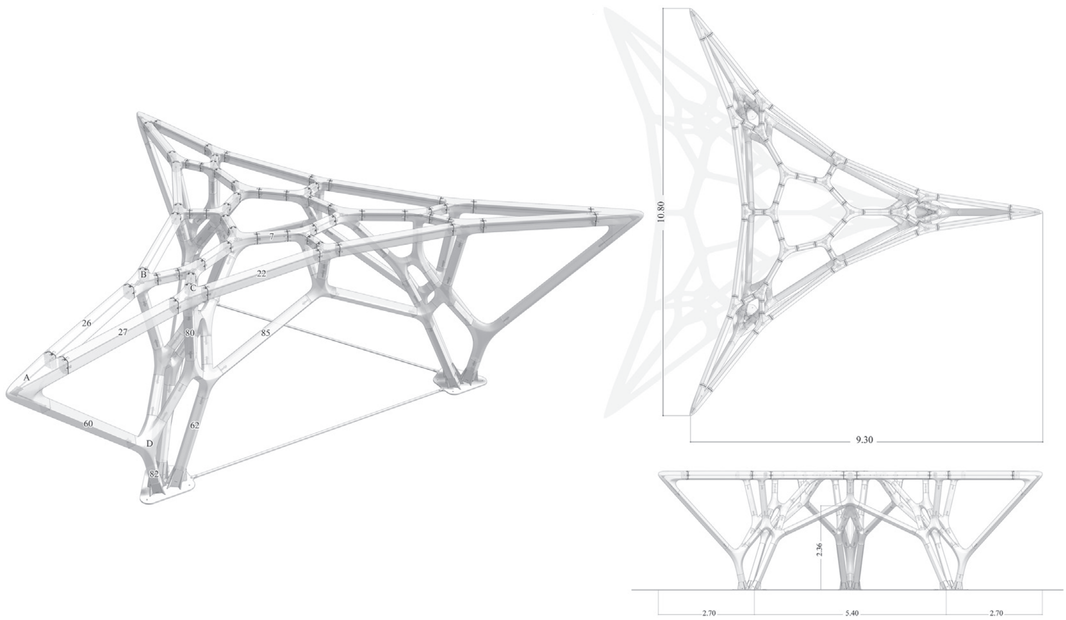

Fig. 3. Plan, elevation and axonometric view of the built structure.

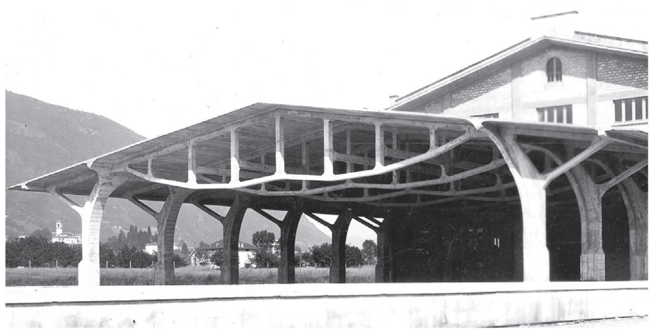

Fig. 4. Chiasso Shed designed by Robert Maillart in Ticino canton, Switzerland, from 1923 to 1925.
Source: Image courtesy of ETH-Bibliothek Zürich).

2.1. Constrained 3DGS model

In order to precisely control the location of supports and the magnitudes of the lateral loads, constrained form and force diagrams were constructed using procedural 3DGS in a parametric environment [2]. In the first step, the global equilibrium was established by constructing the GFP; all vertically applied forces were replaced by a single resultant force $\mathbf{f}_R$ and the directions of the reaction forces in the supports were found by choosing a point on the line of action of $\mathbf{f}_R$ (Fig. 5a). Note that the laterally applied forces $\mathbf{f}_h$ also intersect the line of action of $\mathbf{f}_R$. Moreover, each force $\mathbf{f}_h$ is coplanar with a reaction force and $\mathbf{f}_R$, due to planarity constraints of the reciprocal polyhedral diagrams [5]. By putting planes perpendicular to the direction of the applied loads, we constructed a closed GFP for these boundary conditions. Accordingly, the magnitude of the reaction forces was found (0.35 kN) with respect to the total applied force $\mathbf{f}_R$ (1 kN).

2.2. Subdividing GFP

Subdividing GFP is a design technique that allows exploring a variety of topologically different compression-only forms for a given boundary conditions [6]. In this technique, the internal space of GFP is subdivided into closed, convex polyhedral cells to ensure nodal

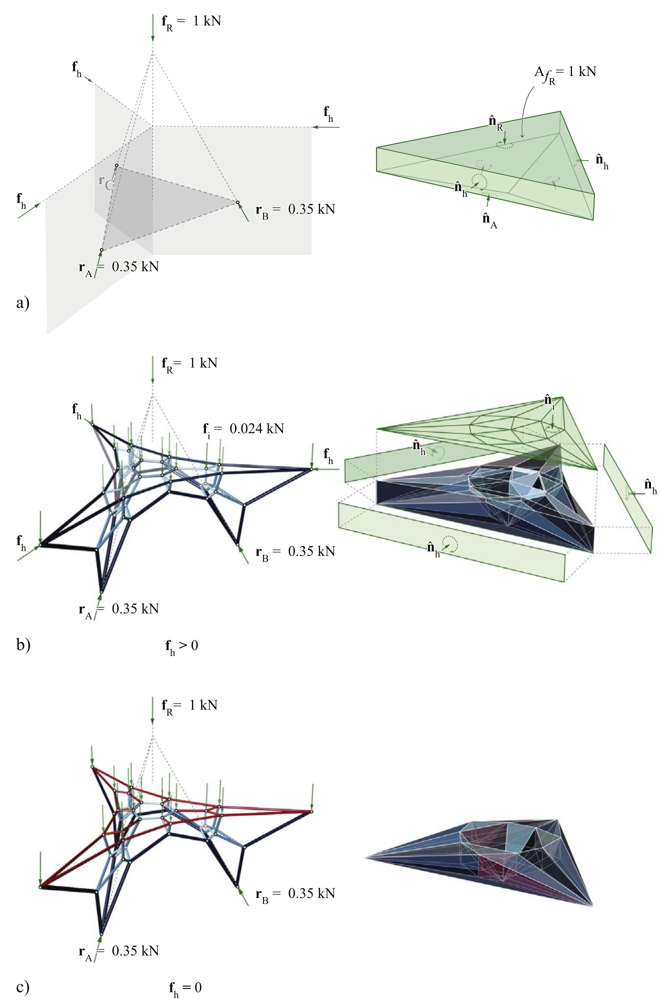

Fig. 5. Construction of the constrained 3DGS model; (a) establishing the global equilibrium and the equilibrium of external forces; (b) subdividing the global force polyhedron and extracting the constrained, compression-only structure; and (c) removing the lateral forces in the boundary condition to get the compression-and-tension-combined.

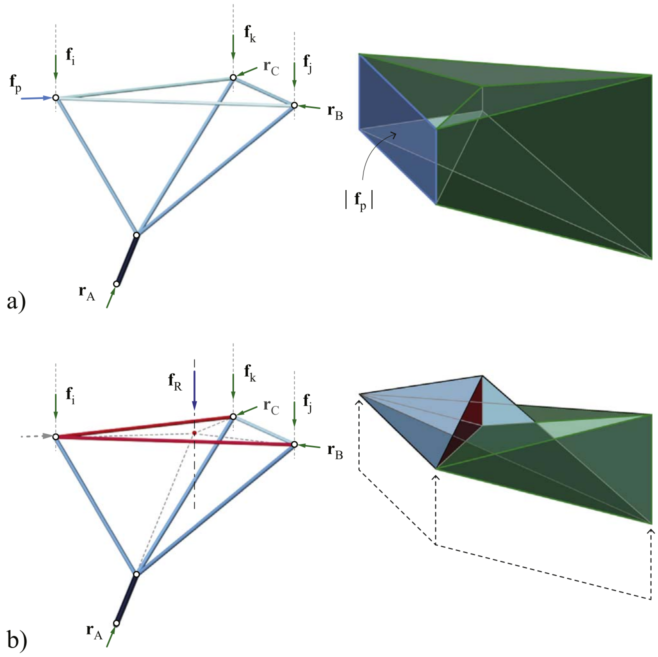

Fig. 6. (a) Compression-only form and force diagrams including convex NFPs; and (b) form and force diagrams with mixed compression and tension forces as a result of subtracting the force f_p.

equilibrium for a compression-only form constrained to the boundary conditions.

Once the global equilibrium was established and the GFP was constructed, its internal space was subdivided into convex polyhedral cells to derive a compression-only spatial structural from, constrained to the given boundary conditions (Fig. 5b). Various subdivision schemes were developed from which the chosen topology of the structure of Hedracrete was selected.

2.3. Manipulating GFP

Graphic statics allows us to produce funicular concepts with both compression and tension members only by manipulating GFP; a designer can start with a GFP that encompasses multiple convex NFPs and later change the GFP to get a form with both tension and compression members. For instance, Fig. 6 illustrates a compression-only structural form and its GFP including 4 convex NFPs. Decreasing the magnitude of the force $\mathbf{f}_p$ in the boundary condition by changing the area of its corresponding face in the force diagram, causes two of the NFPs to become non-convex (complex/self-intersecting). Consequently, the direction of the internal forces within members changes and the resulting structural form will have both compression and tension members (Fig. 6b).

The same technique was used in the 3DGS model of Fig. 5b; the laterally applied loads $\mathbf{f}_h$ were removed from the system by changing the area of their corresponding faces to zero in the force diagram. The resulting design is a funicular form with both compression and tension members where tensile forces on the top chord are supported by compression-only members on the bottom (Fig. 5c).

2.4. Designing and materializing members

The magnitude of the forces in the force diagram is a relative term, for the geometry of the force polyhedron can be scaled proportionally without changing the direction of its faces. The resultant of the applied forces on the structure $\mathbf{f}_R$ is assumed to be 1 kN which provides a proper benchmark for the magnitude of the internal forces. If so, the sum of the areas of the top faces in the force diagram is 1 kN, and the magnitude of each internal force will be divided by the area of the top faces which will be a fraction of one. The minimum feasible dimension for concrete construction without any embedded rebar was the starting criteria for choosing the initial size of the members. The radii of the members were initially chosen from 7.5 to 10 cm based on their internal forces derived from the force diagram.

Table 1
Specifications of the structure.

Type	# of parts	Volume [m^3]	Weight [kg]
Tensile members	30	1.003	1765.28
Compressive members	54	0.911	1603.36
Joints	45	1.2	2112
Heaviest joint	–	0.059	103.84
Heaviest member	–	0.0721	126.896
Total	129	3.114	5480.64

2.5. Matching design loads to reality

The form of the structure is in static equilibrium if it is subjected to the applied loads on its top chord. Since the built structure would not have any predefined applied load on the top, we decided to use the weight of the tensile members as the applied loads keeping the system and the compression members in equilibrium. Therefore, the tensile members were considered to be constructed out of concrete and also sized from 7.5 to 10 cm. The total weight of the tensile members was calculated as 1765.28 kg and the resultant applied force 1 kN was scaled to 17.6 kN to act as the existing applied force on the (Table 1)

For this assumption to be correct, the tributary area for each node on the built structure should be equal to the area of the face corresponding to the applied force on the same node in 3DGS model. Checking the nodal tributary area and the area of the faces of the force polyhedron showed a precise match with a certain tolerance (%0.3 ~ 0.0528 kN) to consider the fabrication and construction imperfections (Fig. 7a, b).

3. Fabrication and assembly

The project's intent was to extend the use of concrete in design and fabrication of discrete spatial systems as opposed to its conventional use as a cast-in-place material. Light-weight Glass Fiber Reinforced Concrete (GFRC) and prefab elements were chosen as the primary material and the construction method for the project. To reduce the self-weight of the concrete, perlite and pumice aggregate were added to the ingredients. To increase the strength of concrete and the tensile capacity, silica fume and chopped glass fibers were also added to the mixture. Considering three axes of symmetry for the form significantly reduced the construction costs and fabrication time of the project; each polystyrene mold, which was milled using a regular three-axis CNC machine, was used three times during the fabrication process.

The connection details were carefully developed to avoid any unnecessary element in the system, and the compressive and tensile members were treated differently; the members carrying compressive forces have a hollow metal tube at both ends to receive their adjacent joints. These simple male-and-female pipe connections increased the precision of the assembly and provided relative stability for the system during assembly obviating the need to use complicated falsework/formwork. There is a dry connection between the compressive members and the joints kept in place due to the axial compressive force in the members after completion (Fig. 8).

The tensile members, on the contrary, include a rebar (d = 12 mm) that is connected to two steel plates (t = 4 mm) at both ends. These plates transfer the tensile force to the plate of the adjacent joint. In the adjacent joint the tensile force is transferred via a rebar to a custom-cut plate at the center receiving all the tensile forces from adjacent members in precise angles to keep the static equilibrium of the node and the structure (Fig. 9).

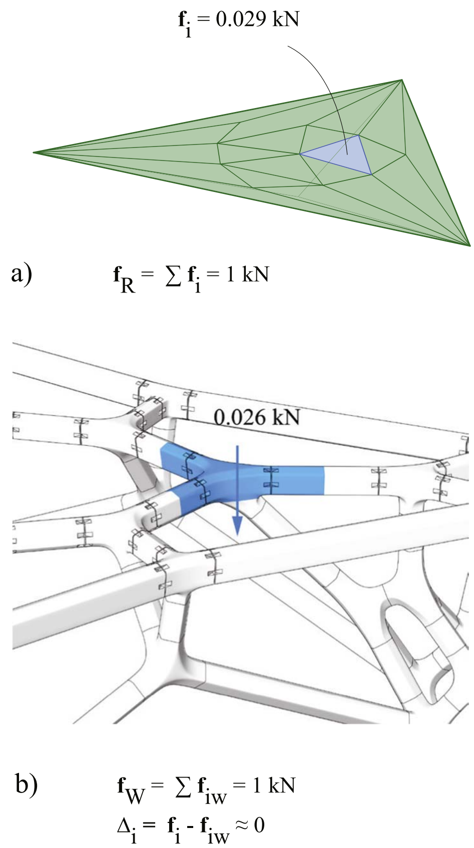

Fig. 7. The negligible differences between the 3DGS design loads (a) and the tributary load per vertex (b).

Fig. 8. The assembly process of the structure; the compression-only parts are simply kept in their position by the use of a male-female detail and the axial force in the members, whereas the tension-only members are kept and connected via bolted plates on the top chord.

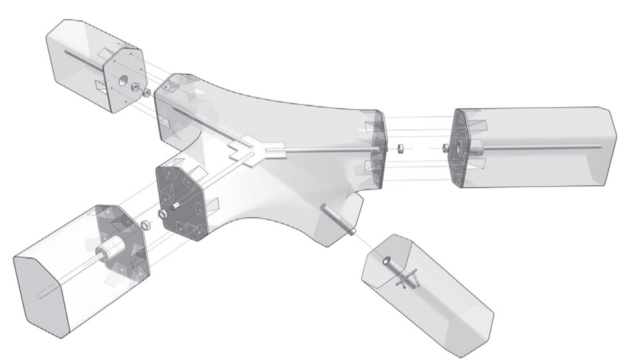

Fig. 9. Exploded axon of a joint with three adjacent tensile members (top) and a compressive member (bottom) revealing the tensile rebars, connecting plates, and the custom cut plate in the center of the joint to receive the rebars with precise angles.

4. Structural analysis

To investigate the mechanical properties of the structure, multiple models with different properties were developed and analyzed under various loading conditions.

4.1. Numerical analysis setups

The following sections will describe the numerical setup for the software as well as the material properties of the project that was used in getting the results.

4.1.1. Used software and their input models

Two commonly used software programs for structural analysis, SAP2000 [24] and ABAQUS6.13 [1], are employed in this study. To validate the equilibrium results of 3DGS, a simplified geometry of the structure was modeled in SAP2000 using linear bar-node elements. The unconfined Mander parametric model and elastoplastic model are used to define the nonlinear stress-strain behavior of steel and concrete. Although SAP2000 can be efficiently used to analyze simplified models with linear elements and prismatic sections, it might not very well predict the failure mechanism of such a complex frame.

The volumetric geometry of the built structure was translated into a triangle mesh in Rhinoceros software [19] and was converted into a tetrahedral mesh in ABAQUS. Both first and second order iso-parametric tetrahedral elements (*C3D4* and *C3D10*) were tested and continuum elements (*C3D10*) were used as the optimum mesh and element type for concrete members in sensitivity analyses. To precisely model the existing structure for analysis purposes, the rebars were also included as truss elements (*T3D2*) in the continuum model. They are embedded into the concrete as smeared-crack elements and do not slide within the concrete. Other parameters such as the linear/nonlinear behavior of concrete, joint fixity, and various loading conditions were set within the software.

4.1.2. Input material properties

Table 2 shows the material properties of steel and concrete that are used as input in SAP2000 analysis. Parameters such as unconfined compressive strength, ultimate strain capacity, and maximum tensile strength of concrete are derived from the compressive strength test on cylindrical specimens (Fig. 10a). Additionally, yield and the final stress and strain of the tested rebars are used to derive the stress-strain curve of Fig. 10b.

Table 2
Mechanical properties of the used materials.

<table>
<tr><th>Material</th><th>Mechanical property</th><th>SAP2000</th><th>ABAQUS</th><th>Unit</th></tr>
<tr><td>Concrete</td><td>Compressive strength, $f_c^{'}$</td><td>23.3</td><td>–</td><td>MPa</td></tr>
<tr><td></td><td>Tensile strength, f_t</td><td>4.3</td><td>–</td><td>MPa</td></tr>
<tr><td></td><td>Modulus of elasticity</td><td colspan="2">22.6</td><td>GPa</td></tr>
<tr><td></td><td>Poisson's ratio</td><td colspan="2">0.2</td><td></td></tr>
<tr><td></td><td>Strain at unconfined compressive strength</td><td>0.002</td><td>–</td><td></td></tr>
<tr><td></td><td>Ultimate unconfined strain capacity</td><td>0.005</td><td>–</td><td></td></tr>
<tr><td></td><td>Final compression slope</td><td>−0.1</td><td>–</td><td></td></tr>
<tr><td></td><td>Mass density</td><td>–</td><td>1760</td><td>kg/m^3</td></tr>
<tr><td></td><td>Dilation angle</td><td>–</td><td>34.0</td><td></td></tr>
<tr><td></td><td>Eccentricity</td><td>–</td><td>0.1</td><td></td></tr>
<tr><td></td><td>Ratio of biaxial to uniaxial yield stress, f_{b0}/f_{c0}</td><td></td><td>1.16</td><td></td></tr>
<tr><td></td><td>Ratio of second stress invariant, K</td><td></td><td>0.67</td><td></td></tr>
<tr><td></td><td>Viscosity parameter</td><td></td><td>0.001</td><td></td></tr>
<tr><td>Steel</td><td>Yield strength, f_y</td><td colspan="2">380</td><td>MPa</td></tr>
<tr><td></td><td>Tensile strength, f_u</td><td>510</td><td>–</td><td>MPa</td></tr>
<tr><td></td><td>Modulus of elasticity</td><td colspan="2">200</td><td>GPa</td></tr>
<tr><td></td><td>Poisson's ratio</td><td colspan="2">0.3</td><td></td></tr>
<tr><td></td><td>Strain at onset of strain hardening</td><td>0.015</td><td>–</td><td></td></tr>
<tr><td></td><td>Strain at maximum stress</td><td>0.11</td><td>–</td><td></td></tr>
<tr><td></td><td>Strain at rupture</td><td>0.17</td><td>–</td><td></td></tr>
<tr><td></td><td>Final slope</td><td>−0.1</td><td>–</td><td></td></tr>
</table>

Table 2 also shows mechanical properties used for modeling steel and concrete in ABAQUS. Defining plasticity characteristics of the materials needs various experimental tests that are beyond the scope of this research. In the absence of such data, the plasticity parameters are determined indirectly by the use of values recommended in the literature [1,11].

Table 3
Compressive and tensile damage parameters of concrete.

Compressive behavior		Tensile behavior	
Inelastic strain	Damage parameter	Cracking strain	Damage parameter
0	0	0	0
0.00035	0.13	0.0003	0.3
0.0006	0.25	0.00045	0.5
0.0013	0.35	0.001	0.7
0.0018	0.41	0.003	0.8
0.0029	0.5	0.005	0.9
0.004	0.55	0.0062	0.99
0.01	0.6		

Table 3 shows damage parameters associated with inelastic strain and cracking strain in ABAQUS: f_{b0}/f_{c0} is the ratio of initial equibiaxial compressive yield stress to initial uniaxial compressive yield stress; K is the ratio of the second stress invariant on the tensile meridian to that on the compressive meridian at initial yield for any given value of the pressure invariant such that the maximum principal stress is negative [1]. Fig. 10c and d shows compressive and tensile stress-strain curves of concrete used in this study. Reinforcing bars are modeled using the same elastic-plastic model as SAP2000 (Fig. 10b).

4.2. Analysis procedures

Various loading scenarios are defined to validate and verify the equilibrium results of 3DGS model (Scenarios 1 and 2), and to understand the effects of fixed joints (Scenario 3) and the self-weight of the

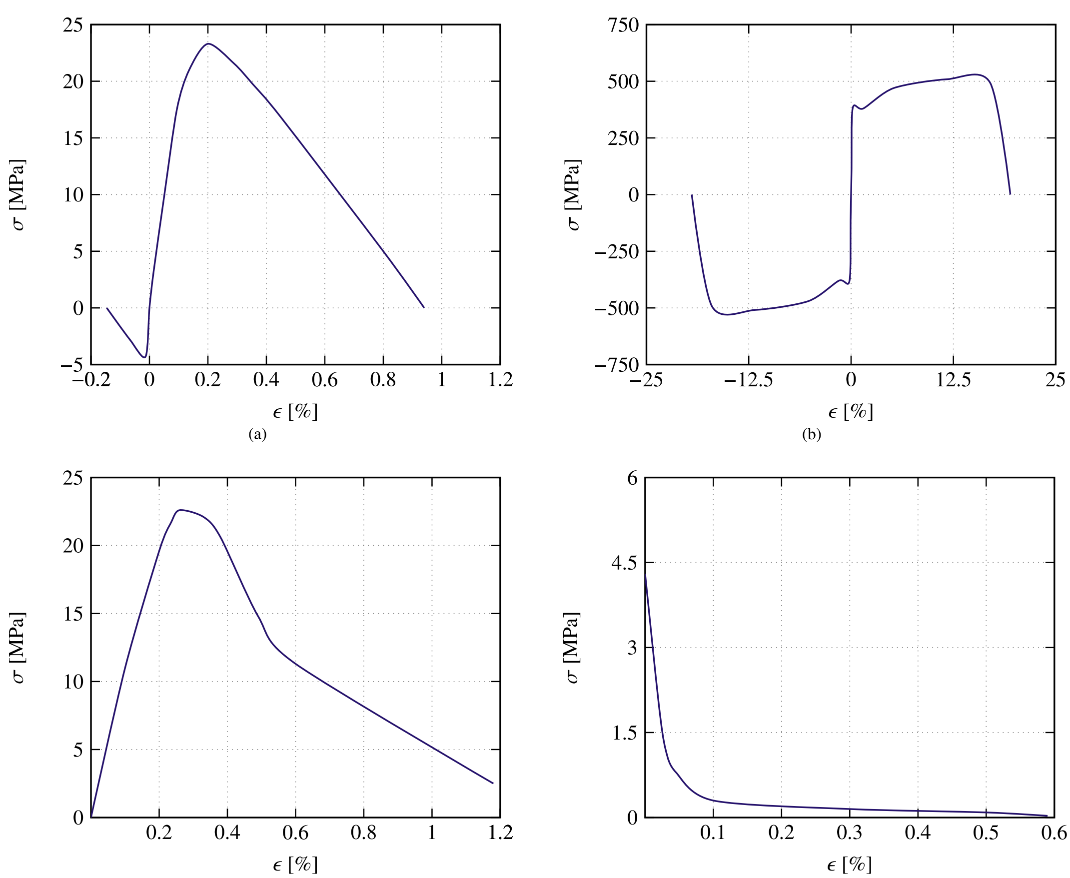

Fig. 10. (a) Compression-tension behavior of concrete in SAP2000. (b) Stress-strain behavior of steel modeled in both software programs. (c) Compressive and (d) tensile behavior of the modeled concrete in ABAQUS.

members on internal stresses (Scenarios 4 to 6). Moreover, more scenarios were considered to study the effect of asymmetrical loading (Scenario 7) and to define the ultimate load-bearing capacity of the structure (Scenario 8). These scenarios are as follows:

- *Scenario 1*: linear model with zero-weight members and hinged nodes under 3DGS design loads;
- *Scenario 2*: linear model with hinged nodes subjected to self-weight of the tensile members;
- *Scenario 3*: linear model with zero-weight members and fixed joints under 3DGS design loads;
- *Scenario 4*: linear model with fixed joints subjected to the self-weight of the members;
- *Scenario 5*: linear model with fixed joints subjected to the weight of the compression members;
- *Scenario 6*: Scenario 5 is subjected to factored 3DGS design loads;
- *Scenario 7*: fixed nodes connected by linear members that subjected to a point load as a critical loading condition; and,
- *Scenario 8*: volumetric mesh model subjected to a point load as a critical loading condition.

Table 4 summarizes all the cases of this study with their corresponding model configurations and their applied loads. Principally, Scenarios 1 to 5 will be used to compare and confirm the results of the 3DGS equilibrium with numerical calculations, whereas Scenarios 6–8 will be used to predict the structural behavior of the system for the loading cases other than the 3DGS design loads.

4.2.1. Scenario 1: analysis under 3DGS design loads

The 3DGS model guarantees static equilibrium of the form under the applied loads that precisely match the area of their corresponding faces in the force diagram (Fig. 5). However, it does not account for the self-weight of the members of the form. Therefore, in the first step, to check the equilibrium results including the internal forces and the reaction forces at the supports, the linear model with zero-weight members was subjected to the 3DGS loads in SAP2000. Moreover, all joints are simulated as hinges with no moment resistance.

The applied loads for each node in SAP2000 are normalized 3DGS design loads and their sum is equal to 1 kN; i.e. the magnitude of each load corresponds to the area of each face divided by the total area of the applied loads. Further, a sensitivity analysis is performed to find the optimum mesh size for the analysis.

Fig. 11a shows the analysis results of SAP2000 for Scenario 1 and the magnitude of the axial forces in the members subjected to 3DGS design loads. All members on the top horizontal chord of the structure are in tension (red) except the six members in the middle with almost zero internal forces, and all the lower members are in compression (blue). The analysis results precisely match the internal forces given by 3DGS method. See Fig. 12 for more details on axial forces in all members.

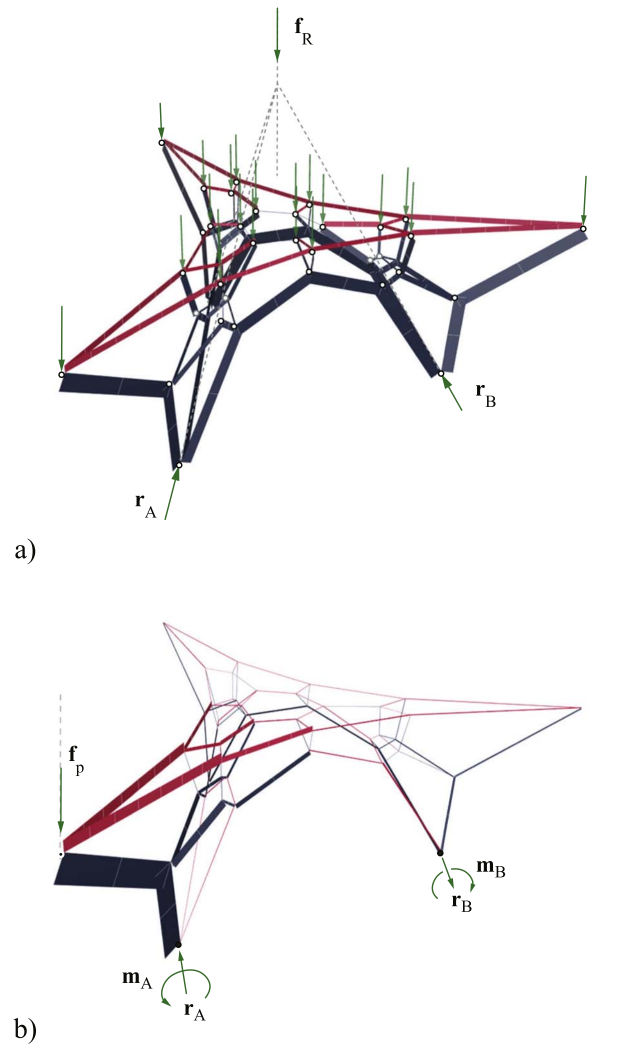

Fig. 11. Axial force of members of structure modeled in SAP2000: (a) under 3DGS loads, (b) under self-weight and concentrated load.

4.2.2. Scenario 2: analysis under the self-weight of the top chord

The structure after construction will not be subjected to any applied loads. Therefore, the tension ties on the top chord are designed such that their self-weight act as the applied loads on the structure, and thus, keep the bottom members and the structure in equilibrium. The tributary area for each node on the top chord, based on the self-weight of the members, is almost equal to the magnitude of its external force in the force diagram (Fig. 7). To check this case the model is analyzed considering the weight of the top members as a dead load with weightless bottom members. Predictably as can be seen from Fig. 12a, b, the results show that reactions and internal forces due to the tributary area of

Table 4
Methodology, details of studied models.

Scenario	Software	Element type	Joint		Self-weight		Load
			Hinged	Fixed	Top	Bottom	
1			◆				3DGS loads
2			◆		◆		–
3				◆			3DGS loads
4	SAP2000	Linear truss		◆	◆	◆	–
5				◆		◆	–
6				◆	◆	◆	Factored 3DGS loads
7				◆	◆	◆	Concentrated load
8	ABAQUS	Tetrahedral			◆	◆	Concentrated load

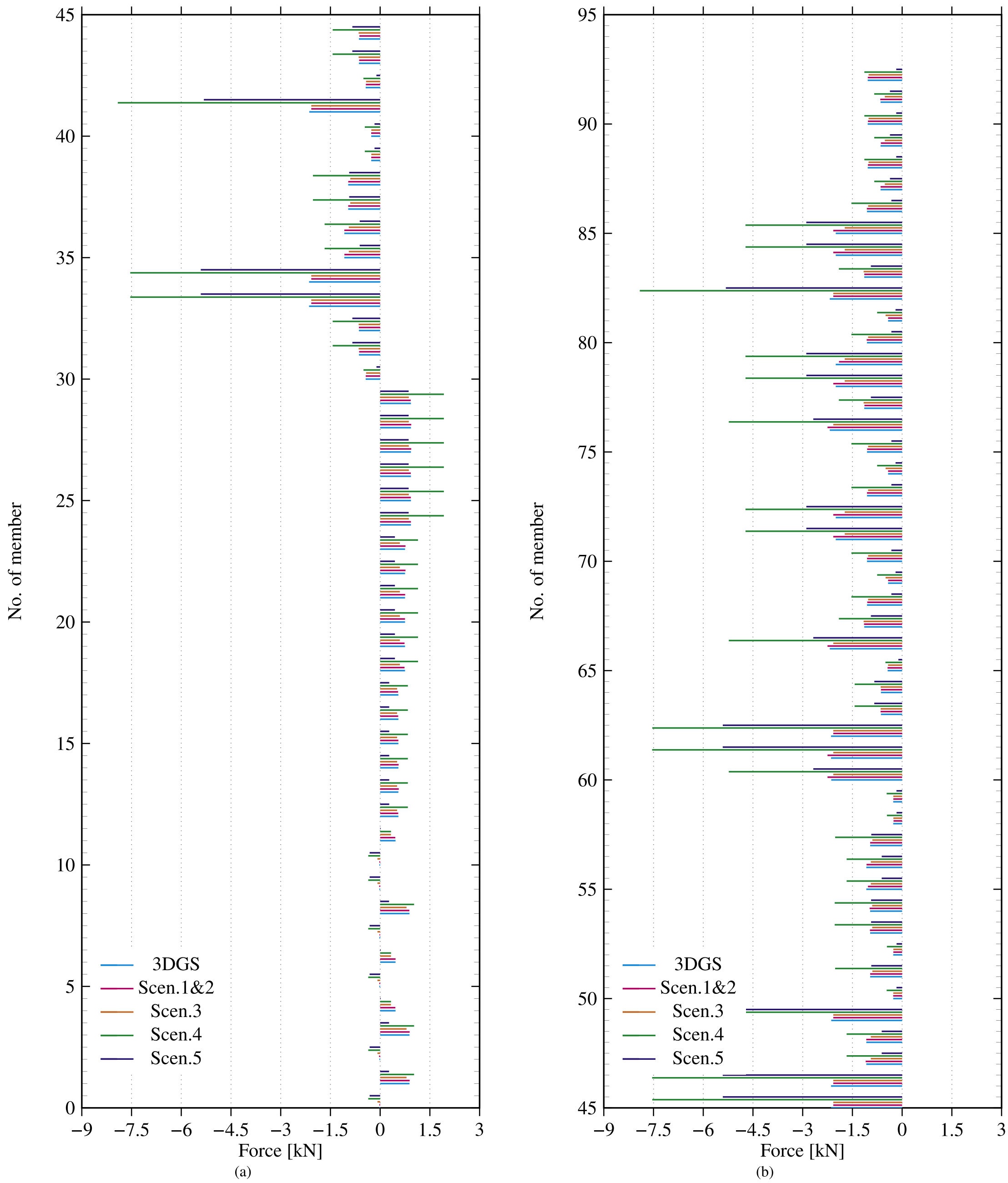

Fig. 12. Comparing internal forces in 3DGS model and Scenarios 1 to 5 in SAP2000: negative values represent members in compression and the positive values represent the tension in members (a) 0 to 44 and (b) from 45 to 93.

each node on the top chord also match the results from the 3DGS design loads. Note that the total 3DGS design load (1 kN) and the total applied force in scenarios 1, 2 and 3 have been multiplied by 1765 (the weight of the top part of the built structure) to allow direct comparison with scenarios involving self-weight.

4.2.3. Scenario 3: fixed joints under 3DGS design loads

Although the structure can be constructed with hinges as originally generated in 3DGS, in practice, it might be subjected to a variety of asymmetric loading cases during its lifetime. Asymmetrical loads in the structure with hinged joints would result in mechanisms since the structure is kinematically indeterminate. Additionally, for the structure with hinged joints to be in equilibrium, it must be subjected to the 3DGS design loads only and the rigidity and stiffness of members should be infinite.

Constructing the structure with moment-resisting joints will significantly improve its performance under asymmetric loading cases. However, in the compression members (with no reinforcement) constraining joints can be problematic because of the low tensile strength of concrete. This was the reason of using fiber reinforced concrete in construction to improve the performance of such members since there is no conventional/traditional reinforcement in these members.

In order to systematically investigate the effect of adding moment-resisting joints to the model, Scenario 1 with fixed joints is analyzed under 3DGS design loads. Results show that on average, internal force of the members decreases by 5%. In fact, adding moment-resisting joints to this funicular form can slightly increase the axial load-bearing capacity of the members subjected to the design loads (Fig. 12a, b).

Although fixing joints creates moments, stress analysis under this loading condition shows that the maximum tensile stress is almost zero and all bottom members are still compression-only. After this verification step, the model is used to investigate the effect of self-weight and

Table 5
Maximum tensile and compressive stress in all scenarios.

	Top members				Bottom members			
Scenario	σ_t [MPa]	#	σ_c [MPa]	#	σ_t [MPa]	#	σ_c [MPa]	#
1	3.78e−3	27	–	–	–	–	− 4.5e−3	60, 76
2	3.7e−3	27	− 0.2e−3	9	–	–	− 4.5e−3	60, 76
3	6.8e−3	14, 16	− 5.2e−3	0	4.8e−3	75, 80	− 0.122	75, 80
4	0.826	24–29	− 0.674	24 − 29	0.388	74, 81	− 0.534	60, 76
5	0.075	14, 16	− 0.053	1, 3, 8	0.298	60, 66, 76	− 0.408	60, 66, 76
6	4.04	14, 16	− 3.011	0, 2, 9, 10	4.3	75, 80	− 7.39	75, 80
7	4.27	26	− 2.82	7	4.3	80	− 6.59	80
8	25.2	26, 27	− 20.4	14, 15	4.3	60	− 23.3	82

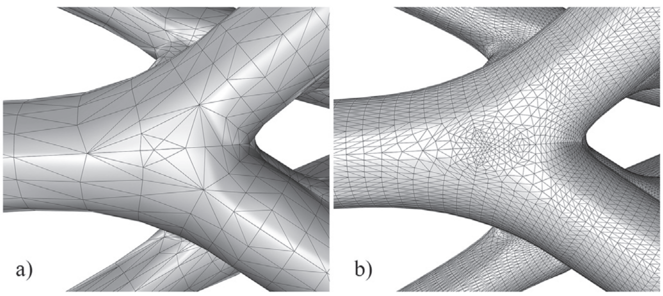

Fig. 13. Mesh densities of the ABAQUS model (a) single subdivision and (b) multiple subdivisions.

also other loading scenarios on the mechanical behavior of the structure that will be discussed in the following sections.

4.2.4. Scenario 4: fixed joints with self-weight

To shed light on the effects of self-weight on the internal stresses of the members in the built structure, the linear model with fixed joints is analyzed with the self-weight of all its members with no external loads. The maximum tensile stress due to the self-weight in the bottom part of the structure occurs in member numbers 74 and 81 and is 0.388 MPa (Table 5). Maximum axial load and deflection occur in member 82 and joint A from Fig. 3. The maximum displacement of joint A is 0.066 mm which is significantly smaller than the projected length of the cantilever part of the structure from the support to the joint A divided by 360 (2700/360 = 7.5 mm). Note that in this loading condition, there are internal moments in the system, and therefore, each bottom member has both tensile, σ_t, and compressive stresses, σ_c (Table 5).

4.2.5. Scenario 5: fixed joints with self-weight of compression-only members

One might suggest a design for a self-supporting structure with steel bars at the top chord instead of the reinforced concrete members. Therefore, Scenario 5 is a speculative case where the weight of the top chord is negligible compared to the self-weight of the bottom members. The analysis results show a little bit of improvement in maximum tensile stress, σ_t in all members, for instance, it reaches to 0.298 MPa in member 60, 66 and 76 which is smaller than the tensile strength of concrete (f_t = 4.3 MPa). In addition, maximum deflection in joint A is 0.03 mm that is almost half of the maximum deflection in Scenario 4. These results suggest that removing the self-weight of the top chord might, in fact, improve the structural performance of the system by reducing the tensile stresses.

4.2.6. Scenario 6: fixed joints subjected to incremental loading 3DGS design loads

The geometry of the form designed by 3DGS is technically considered as the spatial thrust network for the assigned volumes of the members. It is always valuable to predict the maximum strength of the structure based on the design loads. Thus, in this Scenario, the behavior of structure will be evaluated under factored design loads to find its strength capacity in multiple steps. In each step, 3DGS design loads are successively scaled by a constant factor and maximum tensile stress and deflections are calculated and then compared with the maximum tensile stress of concrete and allowable deflection for each member of the structure.

Based on this analysis, the maximum load the structure can take is 1000 kN, and its maximum deflection will be 1.56 mm occurring in joint A. Under such loading condition, members 75 and 80 reach their maximum tensile strength. In fact, 3.1 m^3 of unreinforced concrete that is deliberately distributed in a 50 m^3 of space can take up to 1000 kN of distributed loads – this makes the ratio of the maximum load to the total weight of the structure approximately 19 (102 tons/5.5 tons ≈ 19). The very same analysis is performed for the structure with hinged connection instead of fixed connection to check the maximum strength for the factored 3DGS design loads and results show that the structure is able to carry maximum 1000 kN. Constraining connections reduces the maximum uniformly distributed factored design loads that the structure can take on the other hand, it enhances the performance of the structure in unsymmetrical loading scenarios. Although initially all joints are designed as hinged connections to let the bottom parts act as compression-only members, eventually in the built structure there are constrained joints instead which introduced tensile stresses in these members.

Table 6
Sensitivity analysis.

Designation		Mesh size		Element type		Material behavior		No. of elements	No. of nodes	Element edge length (mm)	
Model name	Model no.	Coarse	Fine	Linear	Quadratic	Linear	Non-linear			Min.	Max.
A	1	4 * ◆		◆		◆		4 * 60,952	2 * 15,121	4 * 8	4 * 500
	2			◆			◆				
	3				◆	◆			2 * 101,269		
	4				◆		◆				
B	1		4 * ◆	◆		◆		4 * 405,303	2 * 86,260	4 * 2	4 * 132
	2			◆			◆				
	3				◆	◆			2 * 618,006		
	4				◆		◆				

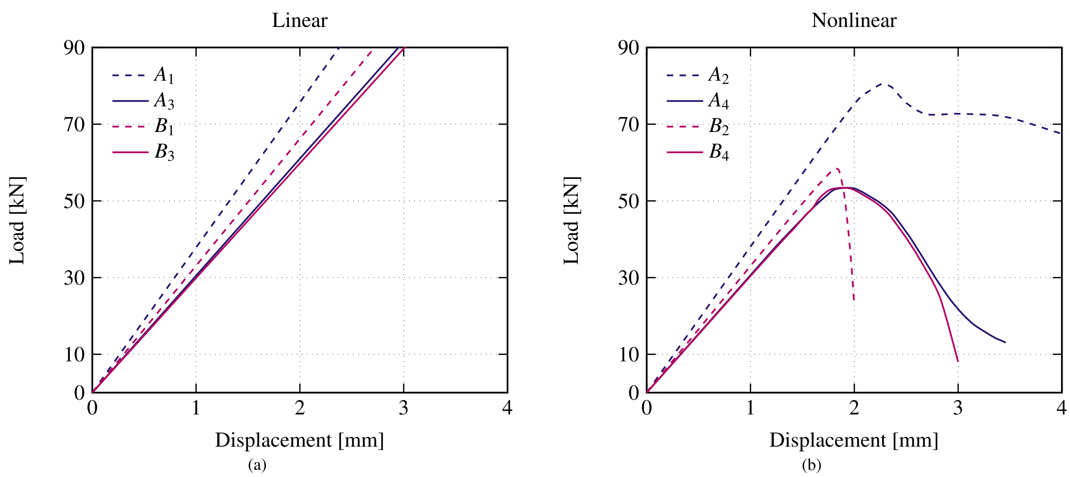

Fig. 14. (a) Linear and (b) nonlinear behavior of different models in ABAQUS.

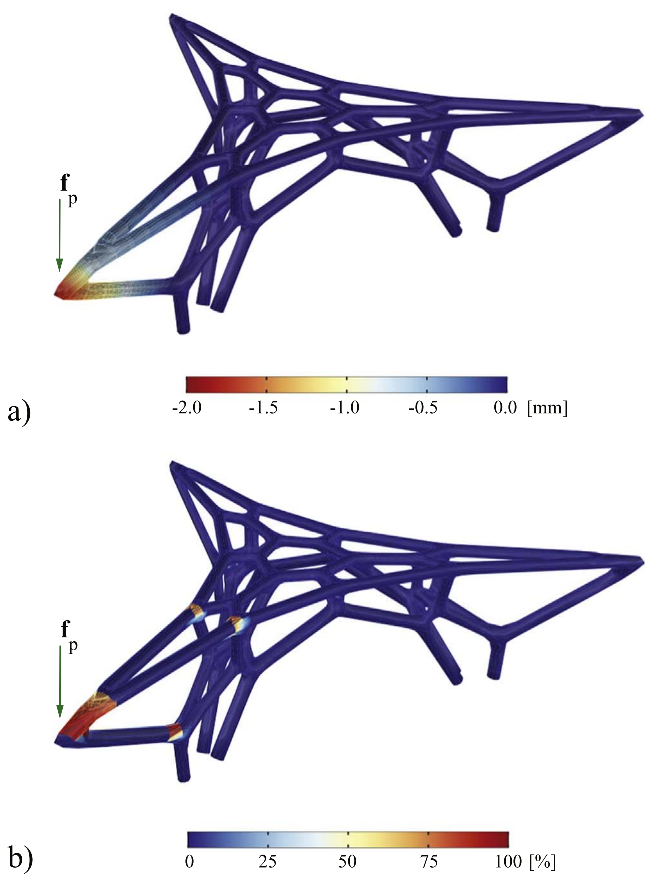

Fig. 15. Analysis outputs; (a) displacement, (b) tensile damage.

Although the structure shows an outstanding performance under the design loads, its behavior must be further evaluated under critical loading conditions. Presumably by evaluating the actual joint stiffness, because, in reality, they will be neither hinge, nor fully fixed, but something in between.

4.2.7. Scenario 7: fixed joints under critical loading condition

In this section, the behavior of the structure is evaluated under an asymmetric loading scenario. Various loading combinations were tested among which a point load at the joint A was chosen as the critical loading condition based on the configuration of the structure. Initially, a 9.81 kN (1 ton) point load is applied at the joint resulting in 0.39 mm deflection in the joint and the maximum tensile stress of 1.54 MPa in member 80. It should be mentioned that all analyses are performed based on the assumption that members are connected together continuously and there is no discrete element.

Gradually increasing the magnitude of the applied force increases the maximum tensile stresses in the members to reach concrete's maximum tensile strength (f_t). Ultimately, the structure can take a point load as large as 14.71 kN (1.5 tons) with maximum deflection 0.55 mm where a local failure occurs in member 80 (Fig. 11b).

Conservatively, in this study, the global failure criterion for the structure is considered when the first local failure happens in the system. However, it is not very clear whether the exact local failure causes the global failure in the system or not. Since the failure analysis of the structure is beyond the capability of SAP2000 program, a more detailed structural model should be analyzed under the critical loading condition, which will be discussed in the following sections.

4.2.8. Scenario 8: failure analysis for volumetric mesh model

The concrete damage plasticity (CDP) model available in ABAQUS is used to simulate the linear and nonlinear behavior of concrete. Crack in tension and crushing in compression are the main failure modes of CDP and these damages can be separately tracked from micro to macro sizes. CDP model assumes that the uniaxial compressive and tensile response of concrete is characterized by damaged plasticity.

4.2.8.1. Sensitivity analysis. For this study two different mesh models were developed; model $A_{1–4}$ with a coarse mesh, and model $B_{1–4}$ with fine mesh (Fig. 13). Each model is analyzed with linear (4 points) and quadratic (10 points) tetrahedral elements for linear and nonlinear material behavior (Table 6). In summary, 8 static analyses are performed to rigorously compare the results.

Although mesh refining results in a more accurate response, investigating the mechanical behavior of the refined model is computationally much more expensive than the investigation on the model with the coarse mesh. To find the effect of the mesh size on the results, multiple linear analyses were performed on the fine and the coarse model to identify a possible convergence in the results (Fig. 14a). Initial linear analyses show that using elements with quadratic (higher order) in both coarse and fine mesh model, A_3 and B_3, has the same effect on the load-displacement behavior of the structure. Therefore, there is no need to use a model with a finer mesh.

4.2.8.2. Final load-displacement curve. Based on the results of the sensitivity analysis, the load-displacement curves converge for models B_4 and A_3, and since B_3 has a finer mesh, it can describe the mechanical behavior of the structure more accurately. The same model will also be

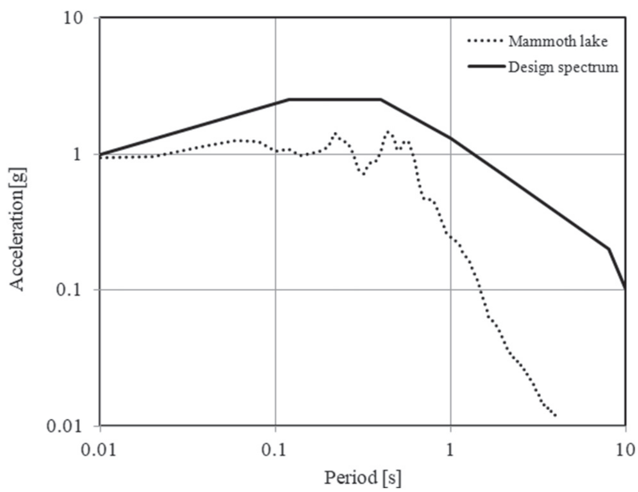

Fig. 16. Response spectrum; (a) design, (b) Mammoth lake.

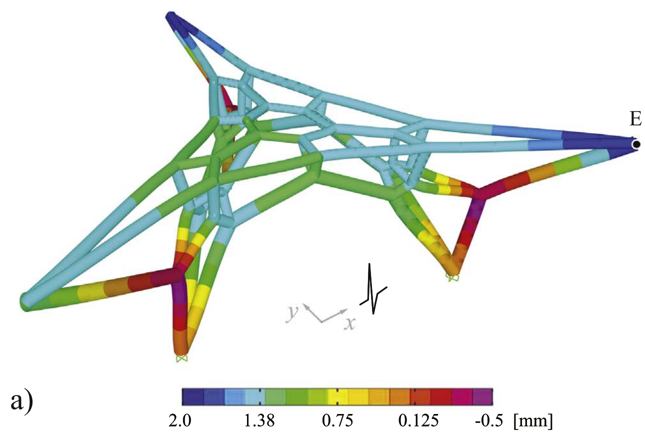

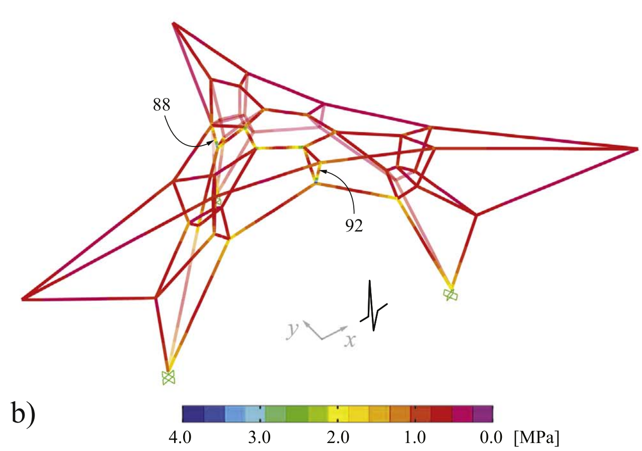

Fig. 17. Dynamic analysis outputs; (a) envelop displacement contour, (b) envelope tensile stress.

used to find the ultimate capacity of the structure under the critical loading condition. Figs. 14b and 15a show the maximum displacement 2 mm under the point load 52 kN (5.3 tons) applied at the joint *A*.

The maximum load and displacement are significantly larger than the results of Section 4.2.7. This, in fact, hints that the first local failure does not result in the global failure of the structure. More specifically, in the critical loading condition, member 80 fails as load increases, but the structure maintains its integrity until the failure of the member 60 occurs. Revisiting the analysis results of the structure in SAP2000 indicates that the maximum load and displacement (14.71 kN (1.5 tons) with maximum deflection 0.55 mm) are much less than the results of ABAQUS (52 kN (5.3 tons) and 1.8 mm). Fig. 15a, b shows the color-coded displacement and tensile damage at the last stage of loading.

5. Dynamic analysis of Hedracrete

The effect of lateral load on the behavior of structure has not been included in the form finding process. Therefore, a post-processing time history analysis is performed to investigate the behavior of Hedracrete under the lateral load. Design spectrum for the structure has been generated based on Iranian code of practice for seismic resistant design of buildings. For the dynamic analysis variety of similar earthquakes to the design spectrum was found through the PEER Ground Motion Database. The horizontal direction of 1980 Mammoth Lake, Long Valley Dam was selected as the most similar earthquake. Both design and selected ground motion are plotted in Fig. 16.

The ground motion record is applied to the structure in the X direction. Displacement and tensile stress of members were progressively monitored during the analysis and results were compared with their maximum allowable to find the location of potential cracks. Envelop displacement contour of Hedracrete (Fig. 17a) along with total time history deflection of critical point E are plotted in Fig. 18. The maximum deflection of the structure is 1 mm.

Plotted stress envelop contour shows that the maximum tensile stress is 4.2 MPa and most of members do not even experience high tensile stress during the earthquake (red members). This is mainly due to low weight of structure and at the same time having high stiffness (modal analysis shows that the natural frequency of Hedracrete is 15 Hz). Tensile strength of vertical members designated as 88 and 92 shown in Fig. 17b with arrows are less than the maximum stress introduced by ground motion and will crack due to the excitation.

6. Structural efficiency: Hedracrete vs. conventional bending frame

Let us assume that Hedracrete was intended to perform as a functioning structure subjected to dead load and live loads. We can propose to cover the top chords of the structure by a layer of structural glass. If so, the dead load for the glass will be 48 kg/m^2, and the live and snow loads will be 196 kg/m^2 and 78 kg/m^2 respectively – following the ASCE 7–10. Therefore, the maximum loading combinations are calculated as 410 kg/m^2. The total area of the top part is 20.5 m^2. Therefore, the structure should be designed for 82 kN resultant force on top instead of the weight of the tensile members 17.6 kN (Section 2.5).

Section 4.2.6 shows that the 3.1 m^3 concrete distributed in 50 m^3 of space in a funicular configuration can transfer 1000 kN to the supports. Simply put, the structure has the factor of safety of 12 for the design load 82 kN.

To highlight the efficacy of the structure, let us design and analyze a conventional reinforced concrete frame with the length, width, and height of 5.4, 2.8, and 3.3 m to cover the same space. The frame should be designed for 410 kg/m^2 (82 kN in total) based on ACI-318 minimum requirements.

A conventional frame satisfying the requirements for covering the same space consists of four beams with the span of 2.8 m, placed 1.8 m apart from each other and subjected to 7.38 kN/m load. These beams sit on two girders with the span of 5.4 m supported by four columns carrying 15 kN load to the ground. Fig. 19a shows a typical cross sections designed to fulfill the requirements for the given design load.

The conventional frame designed for 82 kN design load requires approximately 1.5 m^3 concrete and 163 m rebars in addition to stirrups. Although the concrete volume is less than the volume of Hedracrete, the frame cannot take up to 1000 kN of distributed loads. Therefore, the design of the frame should be updated to provide a better comparison.

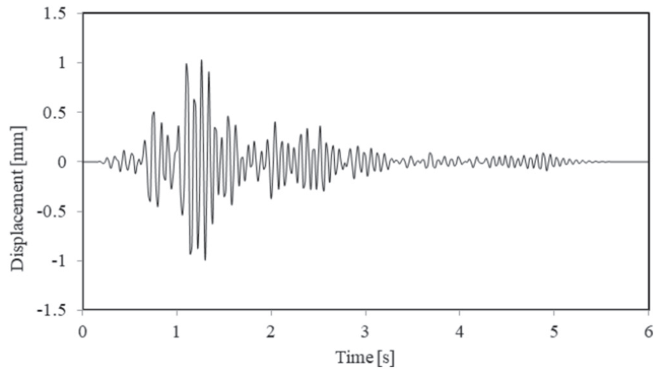

Fig. 18. Displacement history of point E.

As shown in Fig. 19b, the updated frame requires 3.5 m^3 concrete, and 207 m rebar and stirrups which is around %10 and %330 more concrete and steel compared to Hedracrete. This increase in the use of the material is mainly due to the bending moment in the conventional frame that can be avoided by using spatial funicular geometries designed by 3DGS.

7. Summary and conclusions

3DGS allows designers to explore a variety of non-conventional efficient structural forms and control their static equilibrium geometrically. However, the concepts designed by using 3DGS methods do not consider the material properties, and further numerical assessments are required to predict the behavior of the structure under loading conditions other than the 3DGS design loads. In this study, the mechanical behavior of one of the first built funicular polyhedral frames, designed by 3D graphic statics methods, was investigated. The simplified (bar-node) model and a detailed volumetric mesh model of the structure were numerically analyzed under 8 different loading scenarios to understand the mechanical behavior of the system. A series of finite element analysis using SAP2000 and ABAQUS software showed that

- the reaction forces at the supports and the internal forces in the members of the FEM model will precisely match the internal forces of the 3DGS model if the external load on each node of the structure also matches the 3DGS design load; all connections between the members are joints and are free to rotate in 3D space; and all the members are weightless. The reaction and the internal forces in the FEM model will also precisely match the values in the 3DGS if the self-weight of the top members is considered as the only system of

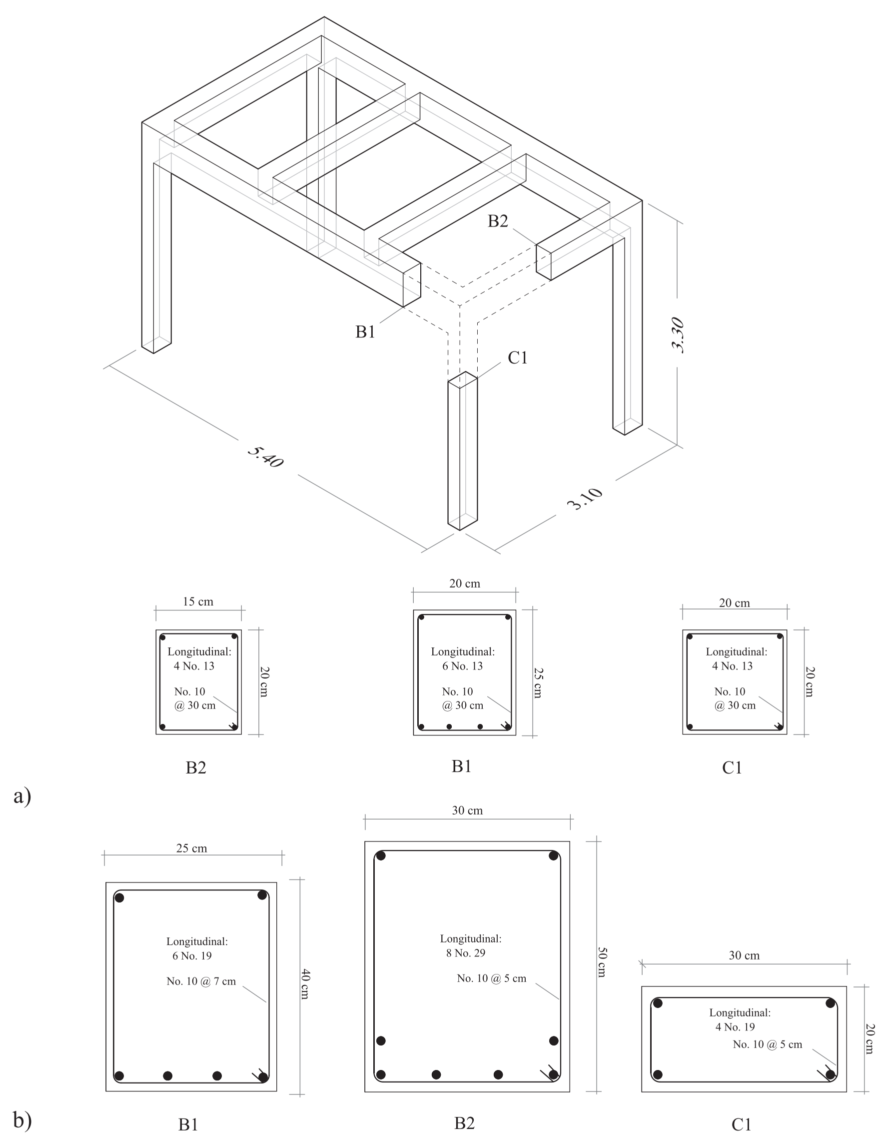

Fig. 19. Section details; a) details based on design loads, b) details based on ultimate load capacity of Hedracrete.

the applied loads on the structure; and the connections are free to rotate;

- although all joints were considered as hinged connections in the 3DGS model, constraining the joints in the FEM model introduced tensile stresses in the compression-only members. This changed the performance of each member from a truss element to a beam element and reduced the maximum uniformly-distributed, factored-design loads that the structure can take. However, it enhanced the performance of the structure in asymmetric loading scenarios compared with 3DGS model. In fact, the performance of hinged structure was quite limited due to the formation of the mechanism under any loading scenarios other than the design loads.

- The analysis results from the detailed FEM mesh model showed that the local failure does not necessarily result in the global failure of the structure. This is a valuable finding, since enhancing the tensile capacity of those compression-only members that failed in analysis can significantly improve the overall load-bearing capacity of the structure.
- Dynamic analysis of the structure showed that most of members experience really low tensile stress (< 2 MPa) which is due to the fact that Hedracrete is a lightweight structure and at the same time has high stiffness.

Hedracrete is built by using 3.1 m^3 of fiber-reinforced concrete and 48 m rebar as its only steel reinforcement with a capacity of transferring 1000 kN of external loads to the supports. Comparing the efficiency of the spatial funicular geometry such as the one in this paper with conventional concrete frames is beyond the scope of this article. However, a simple comparison showed that a conventional frame with the same load-bearing capacity requires more material to compensate the bending moment in the members.

Future studies will include the actual load test of the structure to calibrate the numerical model with the physical model and compare the load-bearing capacity and failure mechanism with the physical examinations. Investigating the efficiency of using spatial funicular prefab systems versus the conventional frame structures to replace outdated infrastructures is a fascinating research topic which authors would like to address shortly.

Acknowledgments

The work presented in this paper was a result of a workshop in 3D graphic statics with 31 participants in collaboration with various material and machining service providers. The authors of the paper would like to thank all the students who worked on the project, people whose hard work and endeavor played a significant role in both design and fabrication processes. We are also thankful to Contemporary Architects Association for organizing the workshop and Sa'adabad Complex officials for hosting the final prototype. The project was partially funded by the Cultural Heritage, Handicrafts and Tourism Organization of Iran, Kheiri Co., Omid Amini and Partners, and Sizan Co. Finally, we would like to express our gratitude to Dr. Diederik Veenendaal for his extremely constructive comments and suggestions on the work and the structure of this paper.

References

[1] Users Abaqus. ABAQUS6.13.. Version 6.13. ABAQUS Inc; 2013.
[2] Akbarzadeh M. 3D graphic statics using reciprocal polyhedral diagrams Ph.D. thesis Zurich, Switzerland: ETH Zurich; 2016.
[3] Akbarzadeh M, Van Mele T, Block P. Compression-only form finding through finite subdivision of the external force polygon. Proceedings of the IASS-SLTE 2014 Symposium, Brasilia, Brazil. 2014.
[4] Akbarzadeh M, Van Mele T, Block P. On the equilibrium of funicular polyhedral frames and convex polyhedral force diagrams. Comput Aided Des 2015;63:118–28.
[5] Akbarzadeh M, Van Mele T, Block P. 3D graphic statics: geometric construction of global equilibrium. Proceedings of the International Association for Shell and Spatial Structures (IASS) Symposium. 2015.
[6] Akbarzadeh M, Van Mele T, Block P. Three-dimensional compression form finding through subdivision. Proceedings of the International Association for Shell and Spatial Structures (IASS) Symposium, Amsterdam, The Netherlands. 2015.
[7] Akbarzadeh M, Mahnia M, Taherian R, Tabrizi AH. Prefab, Concrete polyhedral frame: materializing 3D graphic statics. In: Grohmann M, Bögle A, editors. Proceedings of the IASS Annual Symposium 2017, Interfaces: architecture · engineering · science. Hamburg, Germany. 2017.
[8] Anderson S. Eladio Dieste: innovation in structural art. New York: Princeton Architectural Press; 2004.
[9] Beghini LL, Carrion J, Beghini A, Mazurek A, Baker WF. Structural optimization using graphic statics. Struct Multidiscip Optim 2013;49(3):351–66.
[10] Block P. Thrust network analysis: exploring three-dimensional dquilibrium. Cambridge, MA, USA: Massachusetts Institute of Technology; 2009. Ph.D. thesis.
[11] Bolhassani M, Hamid AA, Lau AC, Moon F. Simplified micro modeling of partially grouted masonry assemblages. Constr Build Mater 2015;83:159–73.
[12] Cremona L. Graphical statics: two treatises on the graphical calculus and reciprocal figures in graphical statics. Translated by Thomas Hudson Beare. Oxford: Clarendon Press; 1890.
[13] Culmann K. Die Graphische Statik. Zürich: Verlag Meyer und Zeller; 1864.
[14] Fivet C, Zastavni D. Key methods from Robert Maillart's salginatobel design process (1928). J Int Assoc Shell Spat Struct 2012;53(1):39–47.
[15] Föppl A. Das Fachwerk im Raume. Leipzig: Verlag von B.G. Teubner; 1892.
[16] Lee J, Mueller C, Fivet C. Automatic generation of diverse equilibrium structures through shape grammars and graphic statics. Int J Space Struct 2016;31(2–4):146–63: http://sps.sagepub.com/content/31/2-_4.tochttp://dx.doi.org/10.1177/0266351116660798.
[17] Lee J, Van Mele T, Block P. Form-finding explorations through geometric transformations and modifications of force polyhedrons. Proceedings of the International Association for Shell and Spatial Structures (IASS) Symposium 2016, Tokyo, Japan. 2016.
[18] Maxwell JC. On reciprocal figures and diagrams of forces. Philos Mag Ser 4 1864;27(182):250–61.
[19] McNeel R. Rhinoceros. 2015. NURBS modeling for Windows: http://www.rhino3d.com.
[20] McRobie A, Baker W, Mitchell T, Konstantatou M. Mechanisms and states of self-stress of planar trusses using graphic statics, part II: applications and extensions. Int J Space Struct 2016;31(2–4):102–11: https://doi.org/10.1177/0266351116660791http://dx.doi.org/10.1177/0266351116660791.
[21] Ohlbrock PO, D'Acunto P, Jasienski JP, Fivet C. Vector-based 3D graphic statics (part III): designing with combinatorial equilibrium modelling. In: Kawaguchi K, Ohsaki M, Takeuchi T, editors. Proceedings of the IASS Annual Symposium 2016 "Spatial Structures in the 21st Century". IASS; 2016.
[22] Rankine WJM. A manual of applied mechanics. London: Griffin; 1858.
[23] Rankine WJM. Principle of the equilibrium of polyhedral frames. Philos Mag Ser 4 1864;27(180):92.
[24] SAP2000 CSI. Computers and Structures Inc., Berkeley, CA, USA. 2013.
[25] Schek HJ. The force density method for form finding and computation of general networks. Comput Methods Appl Mech Eng 1974;3(1):115–34.
[26] Van Mele T, Lachauer L, Rippmann M, Block P. Geometry-based understanding of structures. J Int Assoc Shell Spat Struct 2012;53(174):285–95.
[27] Van Mele T, Mehrotra A, Mendez Echenagucia T, Frick U, Augustynowicz E, Ochsendorf J. Form finding and structural analysis of a free form stone vault. In: Takeuchi T, Kawaguchi K, Ohsaki M, editors. Proceedings of the International Association for Shell and Spatial Structures (IASS) Symposium 2016, Tokyo, Japan. September 2016.
[28] Wolfe WS. Graphical analysis: a text book on graphic statics. New York: McGraw-Hill Book Co. Inc.; 1921.
[29] Zastavni D. The structural design of Maillart's Chiasso Shed (1924): a graphic procedure. Struct Eng Int 2008;18(3):247–52.